# On the fatigue performance of Aluminum alloy 2024 scarfed lap joints

W.Z. Yan*, H.S. Gao[a], X. Yuan[b], F.S. Wang[c] and Z.F. Yue[a]

*Institute of Aircraft Reliability Engineering, School of Mechanics, Civil Engineering and Architecture, Northwestern Polytechnical University, Xi'an 710129, PR China*

**Abstract.**   A series of fatigue test were carried out on scarfed lap joints (SLJ) using in airfoil siding to explore the effect of structural details, such as rows of rivets, lap angles, on its fatigue performance. Finite element (FE) analysis was employed to explore the effect of lap angle on load transfer and the stress evolution around the rivet hole. At last, the fatigue lives were predicted by nominal stress approach and critical plane approach. Both of the test results and predicted results showed that fatigue life of SLJ was remarkably increased after introducing lap angle into the faying surface. Specimen with the lap angle of 1.68° exhibits the best fatigue performance in the present study.

**Keywords:**   fatigue life; scarfed lap joint; lap angle; critical plane approach; finite element method

## 1. Introduction

Over the past decades, many efforts have been dedicated to understanding the fatigue damage of aircraft structure. The reliability of aircraft structure relies on details, such as fillet, bolt and rivet holes (Finney *et al.* 1997). According to statistic, fatigue fracture of fastener holes account for 50-90% of fracture of aging plane (Goranson 1997).

Nowadays, it is a difficult task to predict the fatigue response for Aluminum alloy lap joints (Skorupa *et al.* 2010). Calculation methods as well as design standards are lacked in detail. Most of previous researches were based on experience. Liu *et al.* (2010) has studied the bolt clamping force on the fatigue performance of fastener holes. Carter *et al.* (2006) have studied the effect of various aircraft production drilling procedures on hole quality. The effect of surface processing, such as shot peening (Yang *et al.* 2001), cold expansion (Lacarac *et al.* 2001) on fatigue performance of fastener holes was studied qualitatively. Shankar and Dhamari (2002) studied the effect of oily film corrosion compounds on fatigue behavior of Aluminum alloy 7075 bolted joints.

Previous researches mainly focused on joints with flat jointed sheets (De Rijck *et al.* 2007, Boni *et al.* 2010), which is commonly used in fuselage skin and wing skin. As a novel structure, the

*Corresponding author, Ph.D. Student, E-mail: yanwuzhu24@mail.nwpu.edu.cn
[a]Professor
[b]Ph.D. Student
[c]Associate Professor

scarfed lap joint (SLJ) wherein a lap angle is introduced into the faying surface, has rarely been reported. The design of details and fatigue performance are not available in literature. The SLJ has many advantages over the butt lap joint. The most important feature for SLJ is the lap angle, which has a dramatic influence on its fatigue performance. The lap angle introduced into the faying surface is effective in averaging load transfer of rivets. Consequently, stress concentration around the hole was reduced remarkably.

The present work aimed at optimizing the lap angle of SLJ through a series of tests to achieve the best fatigue performance. Finite element (FE) simulations were carried out to find out the optimal lap angle. The FE results showed a good agreement with the experiment result. At last, fatigue lives with different lap angles were predicted by nominal stress approach and critical plane approach. After optimizing the lap angle, the fatigue life of SLJ was remarkably increased.

## 2. Specimen geometry and the test setup

The geometry of the SLJ specimen is illustrated in Fig. 1. Specimens are constructed of two sheets of clad Aluminum alloy 2024 containing four rows and two columns of fastening holes. The chemical compositions of Aluminum alloy 2024 are presented in Table 1. The faying surface between the two jointed plates was sealed using Aluminum silicone sealant OLV528. Faying surface sealant acts as added substance to reduce the fretting. The fasteners using here are countersunk rivets (YSA302-6-L) and nuts (YSA361-6) which are both made of Titanium alloy.
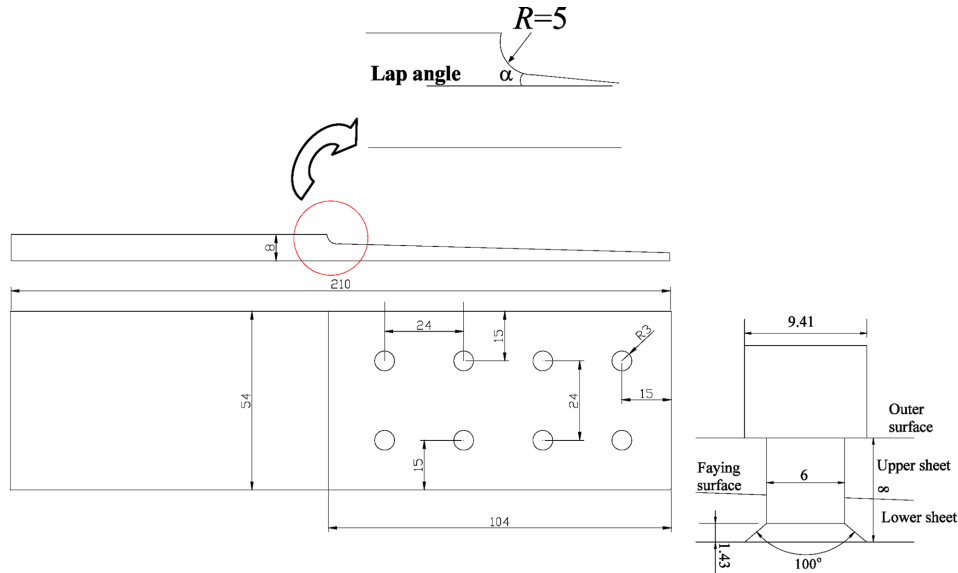


Fig. 1 Geometries of the lap sheet and the countersunk rivet (Unit: mm)

Table 1 The chemical composition of aluminum alloy 2024 used in this work

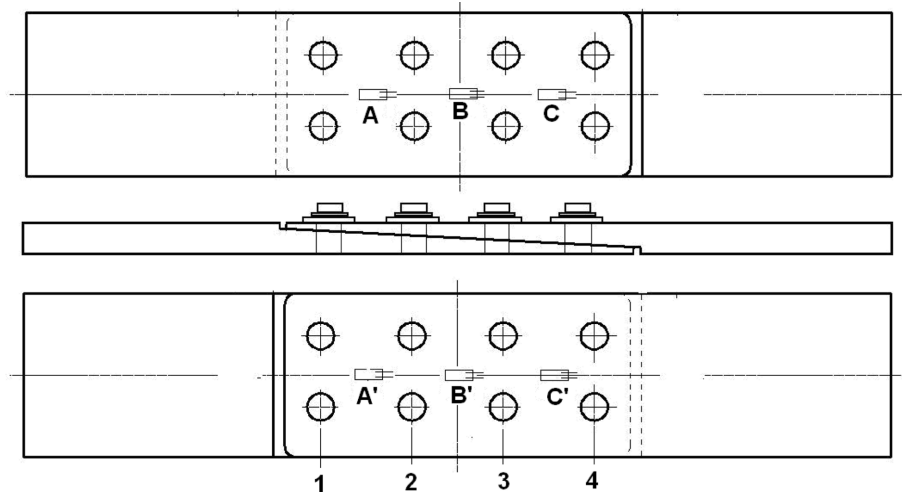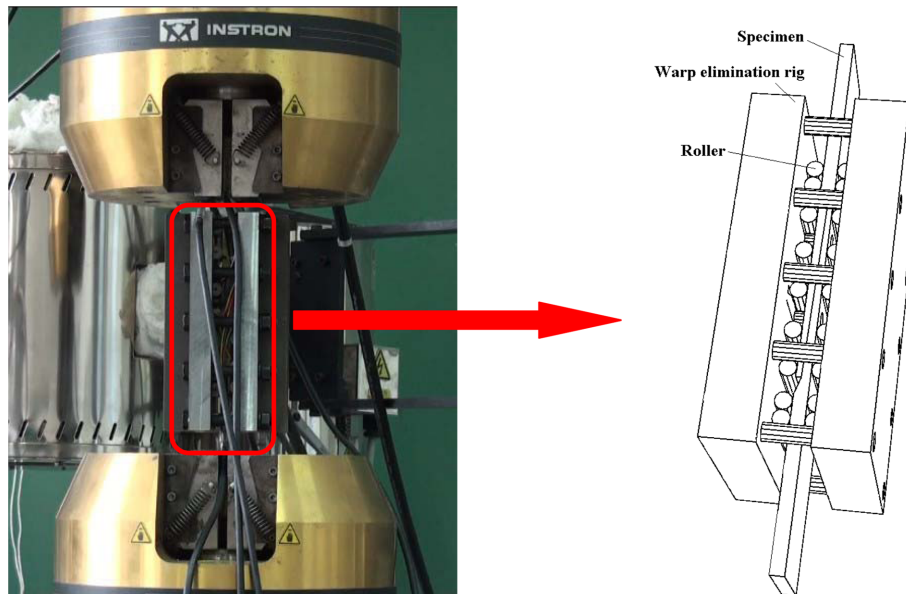| Composition | Al | Cu | Mg | Mn | Si | Fe | Cr | Zn |
|---|---|---|---|---|---|---|---|---|
| Mass fraction | 92.13% | 4.41% | 1.52% | 0.59% | 0.5% | 0.5% | 0.1% | 0.25% |

Fig. 2 Distribution of strain gauges



Fig. 3 Fatigue test setup

The two plates were assembled with rivet clamping force of 5.5 kN and interference of 0.3%. Rivet clamping force was applied by tightening forces in rivet. The interference-fit fastening can minimize the amount of fretting by reducing the relative slip.

Prior to fatigue test, three static tests were performed. The strain gauges were attached in the six positions shown in Fig. 2. After that, all the specimens were tested on a servo-hydraulic fatigue testing machine Instron 8802 (shown in Fig. 3). A specially designed rig was equipped to eliminate the out-of-plane bending via two rows of rollers distributed on the two outer surfaces. The joint panel was fatigue tested at $F_{max}$ = 30 kN, stress ratio of $R$ = 0.06 and a frequency of 4 Hz.

## 3. Experiment

### 3.1 Fatigue life

There were 30 specimens to be carried out by fatigue test. They were classified into 6 groups with respect to lap angles and rows of rivets. Each group contains 5 specimens. The mean fatigue life and coefficient of variation of each group was presented in Table 2.

### 3.2 Fractography

Optical microscope was used to investigate the crack initiation mechanism of the countersunk rivet holes. The specimen fractured at the first row of holes in the lower sheet (refer to Figs. 1 and 2). The possible crack initiation mechanisms include high local stresses, fretting and manufacturing defects created during the riveting process. Fig. 4 shows the fracutre surfaces of the specimens with the lap angle of $\alpha = 1.12^\circ$ (Fig. 4a) and $\alpha = 1.68^\circ$ (Fig. 4b). From Fig. 4(a), it can be seen that crack initiates at the hole bore with a short distance from the faying surface. Fig. 4(b) shows that small evidence of fretting damage can be found at the crack initiation site. The initiation of crack was assisted by the fretting.

## 4. Finite Element (FE) modeling

### 4.1 Model development

In this study, 3D FE model was developed. The ABAQUS/standard finite element package was used to carry out the analysis. Linear hexahedron reduced integration elements, C3D8R (three dimensional eight nodded continuum elements) was used to mesh the model. The FE model and mesh design were shown in Fig. 5. In FE analysis, to gain an optimal result without excessive use of compute time, the mesh was gradually refined as approaching to the hole. The geometry of the model was established as the original size shown in Fig. 1.

In the model, one end of the specimen was fixed and a tensile load of 69.4 MPa was applied on the other end. The clamping forces of all rivets were modeled by applying a "bolt load" (Hibbit *et al.* 2003) of 5.5 kN in the cross section of the rivets. The interference of 0.3% was realized by

Table 2 Fatigue life of specimens with different rows of rivets and lap angles

| Specimen number | Rows of rivets | Lap angle (º) | Fatigue life (cycle) | Coefficient of variation |
|---|---|---|---|---|
| 2110-003 | 4 | 1.68 | 411196 | 0.23 |
| 2110-005 | 4 | 1.10 | 293576 | 0.21 |
| 2110-007 | 4 | 0.55 | 215279 | 0.26 |
| 2110-009 | 4 | 0 | 128527 | 0.18 |
| 2310-003 | 5 | 1.39 | 613804 | 0.30 |
| 2310-005 | 5 | 0.72 | 310475 | 0.27 |

(a) Fracture surface of the specimen with the lap angle of 1.12°



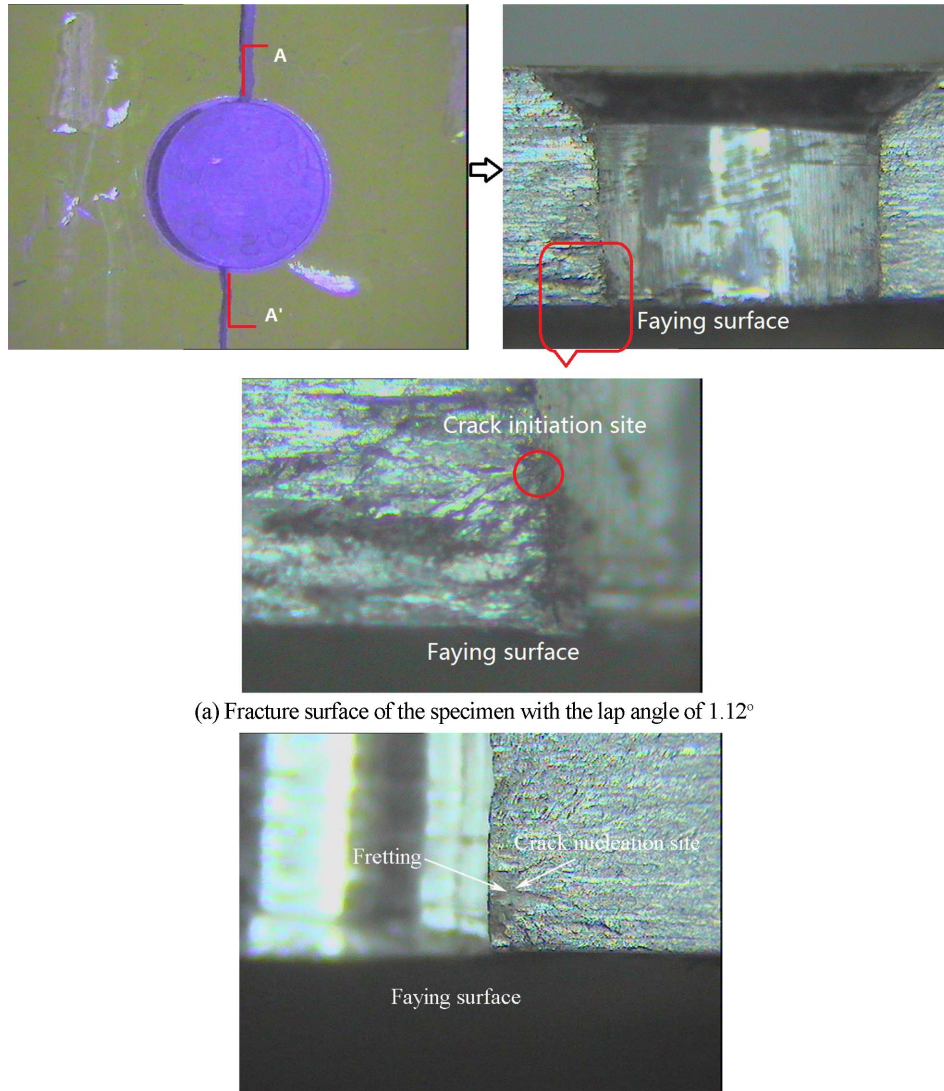(b) Fracture surface of the specimen with the lap angle of 1.68°

Fig. 4 Fracture surface of specimen (lower sheet)

specifying interference fit options that help ABAQUS/Standard resolve excessive overclosure between surfaces in the initial configuration of a model (Hibbit *et al.* 2003). Four contacts were predefined, they are:

  (1) Contact between upper sheet and lower sheet
  (2) Contact between rivets and hole bore
  (3) Contact between collar of countersunk rivet and counter boring
  (4) Contact between nut and upper sheet

For all the contacts, the friction effect was included by using elastic Coulomb friction with $\mu = 0.3$. Small sliding was chosen as the sliding formulation. Surface to surface contact was selected
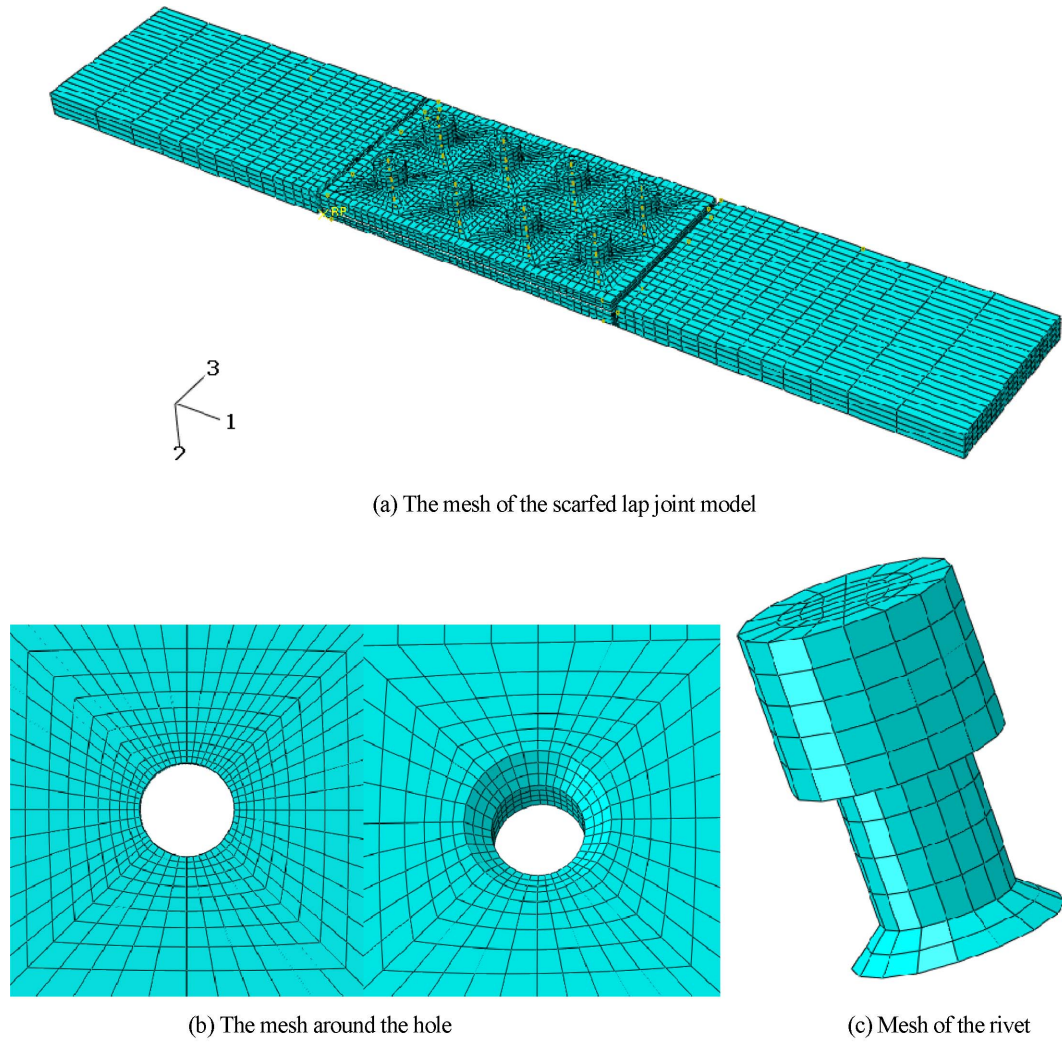
(a) The mesh of the scarfed lap joint model



(b) The mesh around the hole



(c) Mesh of the rivet

Fig. 5 Finite element model for scarfed lap joint

Table 3 Mechanical properties of jointed sheet and countersunk rivet

|                   | Young's modulus (GPa) | Possion's ratio | Yield stress (MPa) | Ultimate strength (MPa) |
|-------------------|-----------------------|-----------------|--------------------|-------------------------|
| Sheet             | 73                    | 0.33            | 350                | 530                     |
| Countersunk rivet | 110                   | 0.35            | -                  | -                       |

as the contact discretization method.

Typical mechanical properties of the material were calibrated by means of the tensile testing and presented in Table 3. In plastic domain, the plastic-flow behavior obeys to a non-linear stress-strain curve

Table 4 Comparison of strains obtained from test and FE results (Unit of strain: $1.0 \times 10^{-6}$)

| Specimen number | Point A | Point B | Point C | Point A' | Point B' | Point C' |
|---|---|---|---|---|---|---|
| 2110-003-1 | 1793 | 1338 | 760 | 768 | 1280 | 1867 |
| 2110-003-2 | 1172 | 1125 | 1027 | 1113 | 1183 | 1314 |
| 2110-003-3 | 1270 | 1088 | 1016 | 1022 | 1204 | 1315 |
| Average value | 1412 | 1184 | 934 | 967 | 1222 | 1498 |
| FE result | 1483 | 1104 | 878 | 873 | 1134 | 1498 |
| Error | 5.05% | 6.75% | 6.03% | 9.85% | 7.21% | 0.02% |

$$\sigma = C\varepsilon^n \tag{1}$$

Where $\sigma$ is the flow stress, $\varepsilon$ is the strain, $C$ is the strength coefficient and $n$ is the strain-hardening exponent.

## 4.2 Model verification

Three static tests were carried out on specimen 2110-003. The measured strains of each point (refer to Fig. 2) were listed in Table 4, and compared with those from FE results. It can be seen that the maximum error is less than 9.85%, which proves that our model is reliable.

## 5. Numerical result

### 5.1 Load transfer mode

The stress concentrations in shear joints are responsible for fatigue damage and crack initiation. The locations of the stress concentrations depend on mode of load transfer. Two load transfer modes were considered in the present work:
(1) The shear force across the rivet midsection,
(2) The friction force between the upper and lower sheets.
The first load transfer mode depends on lap angle, interference fit, hole expansion etc. The second load transfer mode mainly depends on the rivet clamping force (see Fig. 6) and the friction coefficient between the upper and lower sheets.
The pin load distribution for each row of rivets can be expressed by

$$R = p_t / p \tag{2}$$

Where $p_t$ is pin load of each row of rivets, $p$ is total applied load. Fig. 7 shows how the pin load distribution evolves with the lap angle. It can be seen that rivets of row 1 and row 4 (refer to Fig. 2) bear the most of load. However, they decrease with the increase of lap angle. On the contrary, pin load of row 2 and row 3 are much smaller, nevertheless, they increase with the increase of lap angle. Thus, the lap angle averaged the pin load distribution.
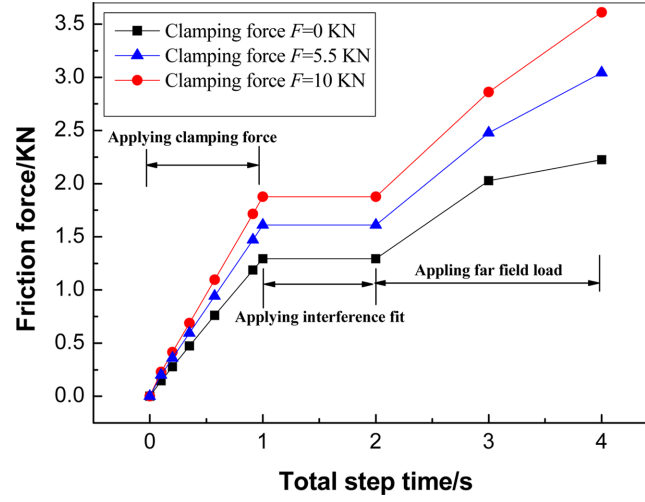
Fig. 6 Effect of rivet clamping force on friction force (four rows of rivets). Lap angle $\alpha = 1.68^{\circ}$
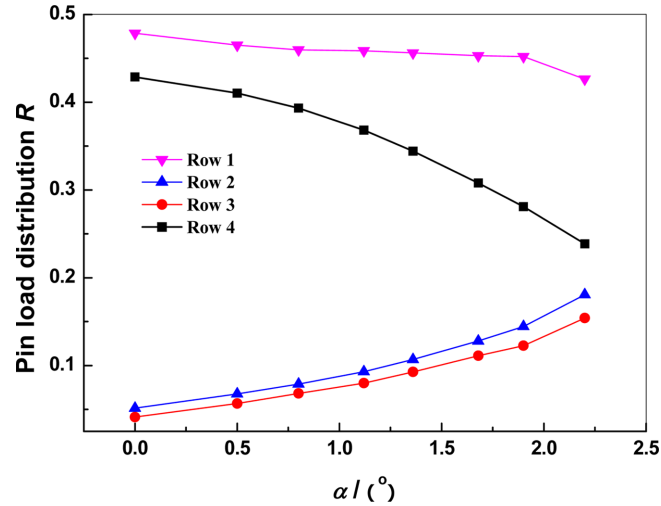


Fig. 7 Effect of lap angle on pin load distribution of each row of rivets (four rows of rivets)

## 5.2 Effect of rows of rivets

A prime feature for lap joint is the rows of rivets. Fig. 8 shows the effect of rows of rivets on pin load distribution and the maximum von Mises stress around the hole. It can be seen that the case with four rows of rivets generates a relatively averaged pin load. However, a larger stress was also observed. Though 5-row configuration generates a lower stress around the hole, the middle row of rivets bear only 2.5% load, which can not make full use of materials. Meanwhile, 5-row configuration increases the weight of airfoil siding, which is not expected in aircraft design. Actually, 4-row configuration can satisfy the design requirement and is preferred.
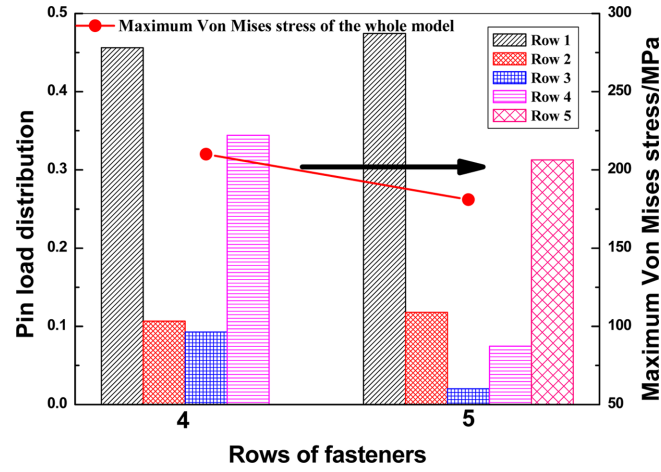
Fig. 8 Effect of rows of rivets on pin load distribution and maximum Von mises stress



(a) $\alpha = 0^{\circ}$



(b) $\alpha = 1.12^{\circ}$



(c) $\alpha = 1.68^{\circ}$
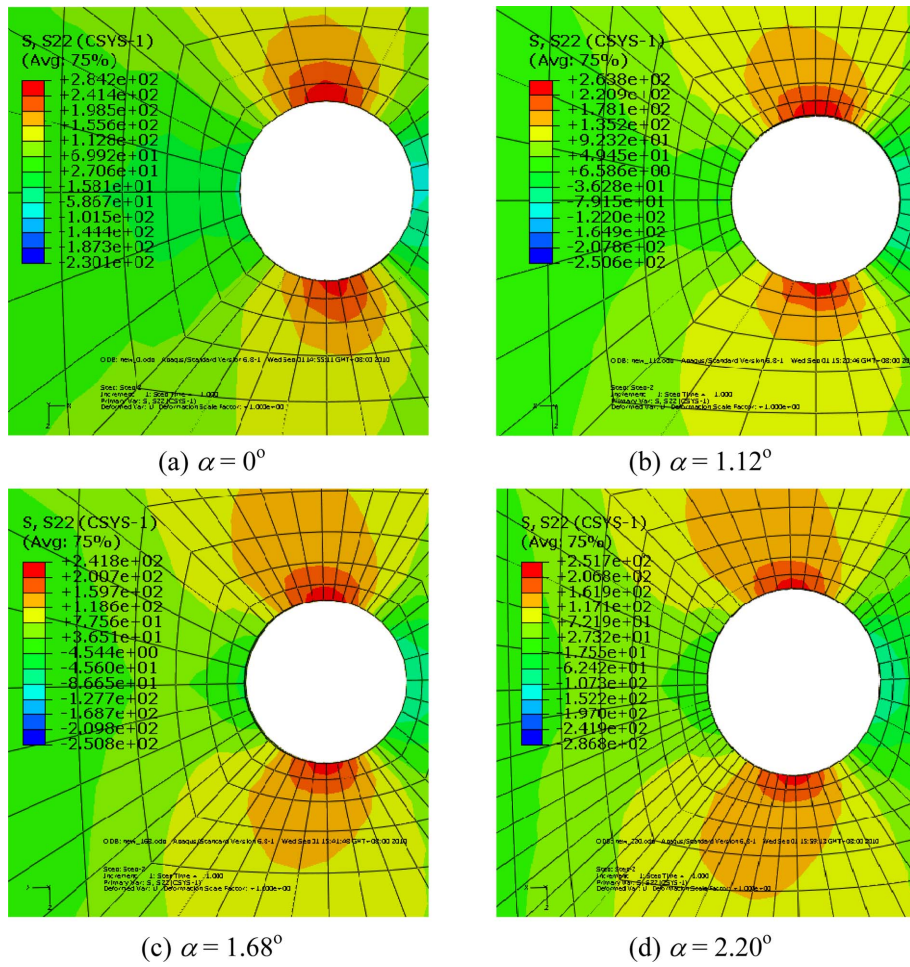


(d) $\alpha = 2.20^{\circ}$

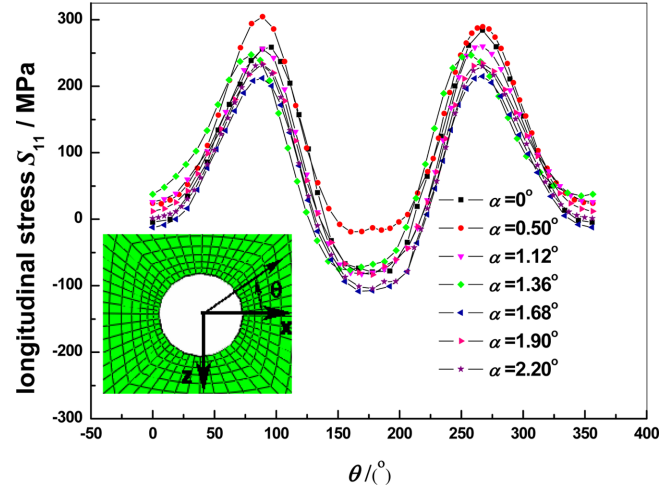Fig. 9 Tangential stress distribution for different lap angles (four rows of rivets)

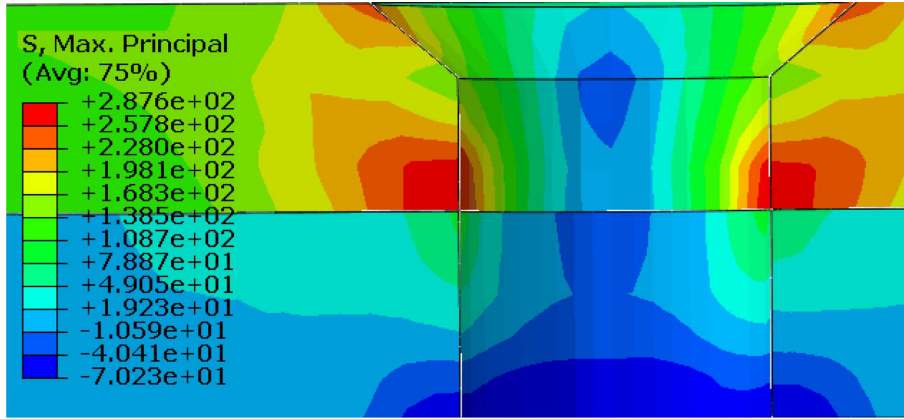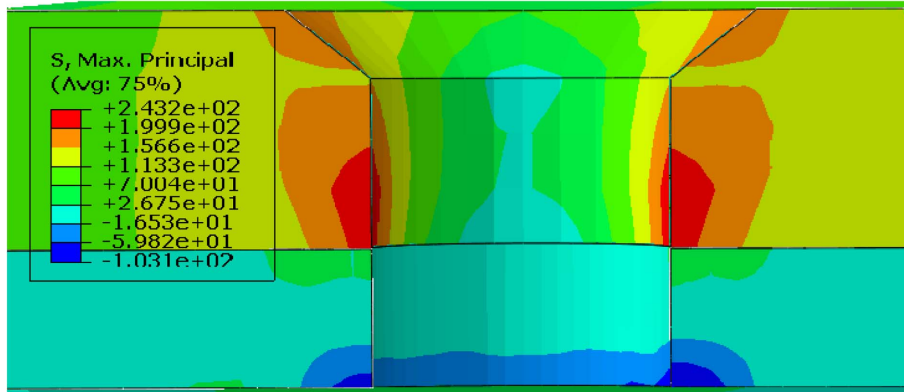Fig. 10 Effect of lap angle on the evolution of longitudinal stress around the hole edge



(a) $\alpha = 0^{\mathrm{o}}$



(b) $\alpha = 1.68^{\mathrm{o}}$

Fig. 11 Stress contour of open hole along $90^{\mathrm{o}}$ direction (refer to Fig. 10)

### 5.3 Effect of lap angle on stress around the hole

It is reported that tangential stress plays an important role in crack initiation of fastener holes (Chakherlou *et al.* 2003). Fig. 9 shows the distribution of tangential stress around the first row of holes (lower sheet) on the faying surface. It is seen that lap angle exhibits a remarkable influence on tangential stress around the hole. This was further illustrated in Fig. 10, which showed that the maximum longitudinal stress occurred in the 90° and 270° directions. The minimum longitudinal stress happened when the lap angle equal to 1.68°.

The max principal stress contour plot along 90° direction (refer to Fig. 10) was shown in Fig. 11. It can be seen that the maximum stress occurs inside the hole bore of the lower sheet with a short distance from faying surface. This is also in consistence with the fractography result. Thus, the mechanism for crack initiation of countersunk rivet hole is that crack is induced by stress concentration although it may still be assisted by the fretting.

### 5.4 Effect of lap angle on cracking behavior of countersunk hole

It is reported that the load transfer ratio has a remarkable influence on the crack initiation locations (Park *et al.* 2007). For the low load transfer countersunk holes, many initial cracks were formed inside the hole bore. However, for the high load transfer countersunk holes, cracks always initiated at the faying surface in the form of corner crack. This phenomenon can be rationalized by the bearing load distribution due to load transfer through rivet. From the analysis in Sections 5.1 and 5.3, we learned that the lap angle reduced the load transfer ratio of the first row of rivets, and the highly stressed site migrated from the faying surface to the middle of the hole bore. This is also in consistence with Park's results (Park *et al.* 2007).

## 6. Fatigue life prediction

### 6.1 Nominal stress approach

As we all know, the stress concentration factor has a remarkable influence on the fatigue life of structures. Zheng (1986) has developed a formula to predict crack initiation life. The new formula reveals a correlation between the fatigue crack initiation life, the notched element geometry, the cyclic loading condition, the tensile properties and the fatigue crack initiation threshold, which is indicated as an important parameter in describing the fatigue damage and crack initiation. This formula can be expressed by

$$N = C_i [\Delta\sigma_{eqv}^{2/(1+n)} - (\Delta\sigma_{eqv})_{th}^{2/(1+n)}]^{-2} \tag{3}$$

$$\Delta\sigma_{eqv} = \sqrt{\frac{1}{2(1-R)}} K_t \cdot \Delta S = \sqrt{\frac{(1-R)}{2}} K_t \cdot S_{max} \tag{4}$$

where $C_i$ is coefficient of crack initiation resistance, which can be obtained by regression method, $\Delta\sigma_{eqv}$ is the amplitude of equivalent stress, $(\Delta\sigma_{eqv})_{th}$ is the threshold value of the amplitude of equivalent stress, $n$ is the strain hardening exponent, $R$ is the stress ratio, $K_t$ is the stress concentration factor, $S_{max}$ is the maximum nominal stress.

Table 5 Fatigue parameters for Aluminum alloy 2024

| Parameters | $b$ | $c$ | $\sigma_f'$ (MPa) | $\varepsilon_f'$ | $s$ | $\upsilon_p$ |
|---|---|---|---|---|---|---|
| Value | -0.124 | -0.65 | 1103 | 0.22 | 0.3 | 0.5 |

Table 6 Stress concentration factor $K_t$ and fatigue lives for different lap angles

| Lap angle (°) | Stress concentration factor $K_t$ | Fatigue life $N$ (Cycle) |
|---|---|---|
| 0.00 | 3.54 | 95883 |
| 0.55 | 3.43 | 183613 |
| 1.10 | 3.27 | 214220 |
| 1.68 | 2.98 | 295286 |

The value of $K_t$ resulting from different lap angles can be obtained from the FE results. The $K_t$ values and the predicted fatigue lives were presented in Table 6. It is seen that the predicted fatigue life increases with the increase of lap angle.

### 6.2 Critical plane approach

#### 6.2.1 Smith-Watson-Topper (SWT) model

Extensive studies have been carried out on the application of fatigue methodologies to predict fatigue life of lap joint (Sum *et al.* 2005, Duprat *et al.* 1996). It is reported that the SWT model achieves better accuracy than other models for high cycle fatigue (HCF) (Ding *et al.* 2007). The SWT model involves both cyclic strain range and maximum stress. It can be expressed as follows (Smith *et al.* 1970)

$$DP_{SWT} = \Delta\varepsilon_a \sigma_{n,\max} = \frac{(\sigma_f')^2}{E}(2N_f)^{2b} + \varepsilon_f' \sigma_f'(2N_f)^{b+c} \tag{5}$$

where $DP_{SWT}$ is the damage parameter, $\Delta\varepsilon_a$ is the amplitude of the normal strain, $\sigma_{n,\max}$ is the maximum normal stress, $\sigma_f'$ and $b$ are the fatigue strength coefficient and exponent, $\varepsilon_f$ and $c$ are the fatigue ductility coefficient and exponent, $E$ is Young's modulus. The fatigue parameters of Aluminum alloy 2024 were presented in Table 5.

#### 6.2.2 Critical plane approach

The transformation of stress and strain with respect to plane angle can be expressed by

$$\sigma_{11}' = \frac{\sigma_{11} + \sigma_{33}}{2} + \frac{\sigma_{11} - \sigma_{33}}{2}\cos 2\theta_i + \tau_{12}\sin 2\theta_i \tag{6}$$

$$\varepsilon_{11}' = \frac{\varepsilon_{11} + \varepsilon_{33}}{2} + \frac{\varepsilon_{11} - \varepsilon_{33}}{2}\cos 2\theta_i + \varepsilon_{12}\sin 2\theta_i \tag{7}$$

$$\gamma_{12}' = \frac{\varepsilon_{11} - \varepsilon_{33}}{2}\sin 2\theta_i - \varepsilon_{12}\cos 2\theta_i \tag{8}$$
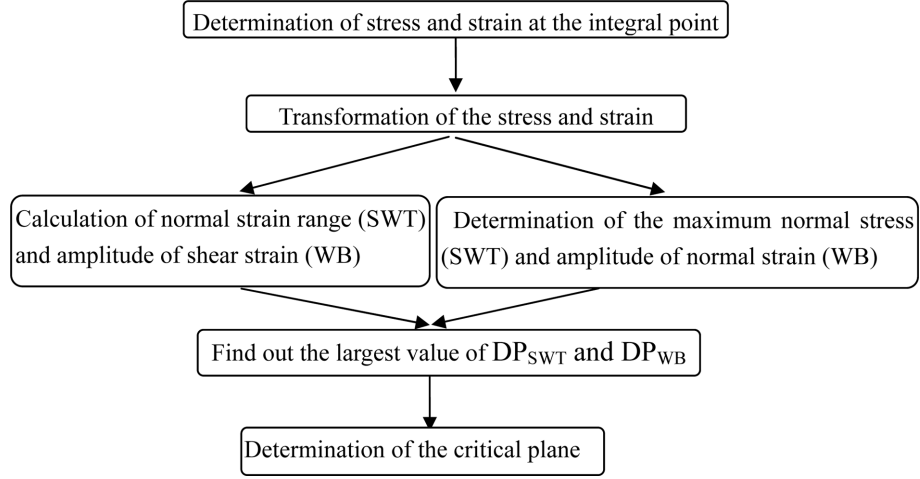
Determination of stress and strain at the integral point

↓

Transformation of the stress and strain

↙ ↘

Calculation of normal strain range (SWT) and amplitude of shear strain (WB)

Determination of the maximum normal stress (SWT) and amplitude of normal strain (WB)

↘ ↙

Find out the largest value of $DP_{SWT}$ and $DP_{WB}$

↓

Determination of the critical plane

Fig. 12 Determination of critical plane and damage parameters for SWT and WB model

(a)
Tested fatigue life/ Cycle
Predicted fatigue life/ Cycle

(b)
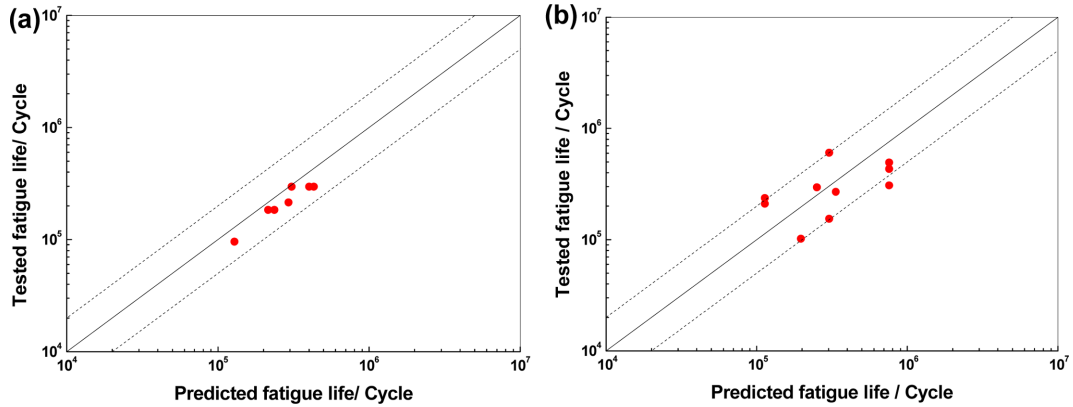Tested fatigue life / Cycle
Predicted fatigue life / Cycle

Fig. 13 Comparison between predicted fatigue lives and experimental fatigue lives. (a) predicted by Zheng's formula, (b) predicted by critical plane approach

Wherein:

$\sigma_{11}, \sigma_{33}, \tau_{13}$ : normal stress and shear stress before transformation,

$\varepsilon_{11}, \varepsilon_{33}, \varepsilon_{13}$ : normal strain and shear strain before transformation,

$\theta_i$ : plane angle ($0^o \le \theta_i \le 180^o$),

$\sigma'_{11}, \varepsilon'_{11}, \gamma'_{13}$ : normal stress, normal strain and shear strain with respect to $\theta_i$,

A special program was prepared to determine the critical plane. The flow diagram was shown in Fig. 12. The value of $\theta_i$ was increased from $0^o$ to $180^o$ with an increment of $1^o$. The normal stress and normal strain of the new plane were then obtained by Eqs. (5)-(7). The plane angle corresponding to the maximum damage parameter can be considered as the critical plane angle.

The predicted fatigue lives was compared with that from test and plotted in Fig. 13. It is seen that most of the data points distribute within the factor-2 scatter band. However, the results predicted from Zheng's (1986) formula shows a better agreement with the experimental results with a lower dispersity.

## 7. Conclusions

The present work aims at optimization of structural details of scarfed lap joint, such as lap angle, rows of rivets. To this aim, a series of fatigue test were performed on specimens with different lap angles and rows of rivets. Finite element simulations were carried out to investigate the effects of structural details on stress evolution around the holes as well as pin load distribution. The nominal stress approach and critical plane approach based on SWT model were employed to predict fatigue life. The following conclusions can be drawn:

(1) Specimens with four rows of rivets achieve best compromise between design requirement and cost.

(2) Lap angle plays an important role in averaging pin load as well as stress evolution around the hole. There is an optimal lap angle exists for scarfed lap joint. Specimen with the lap angle of $1.68^\circ$ exhibits the best fatigue performance.

(3) For scarfed lap joint, fatigue crack initiated at hole bore in the lower sheet with a short distance from faying surface. Crack initiation was induced by stress concentration assisted by the fretting. The application of critical plane approach in fatigue life prediction of riveted hole is doubtful. Fatigue life of riveted holes can be well predicted by Zheng's formula.

## Acknowledgments

## References

Boni, L. and Lanciotti, A. (2011), "Fatigue behaviour of double lap riveted joints assembled with and without interfay sealant", *Fatigue Fract. Eng. Mater. Struct.*, **34**(1), 60-71.

Carter, R.W., Steven, J.W., Toivonen, P., Makeev, A. and Newman, J.J. (2006), "Effect of various aircraft production drilling procedures on hole quality", *Int. J. Fatigue*, **28**, 943-950.

Chakherlou, T.N. and Vogwell, J. (2003), "The effect of cold expansion on improving the fatigue life of fastener holes", *Eng. Fail. Anal.*, **10**, 13-24.

De Rijck, J.M.M., Homan, J.J., Schijve, J. and Benedictus, R. (2007), "The driven rivet head dimensions as an indication of the fatigue performance of aircraft lap joints", *Int. J. Fatigue*, **29**, 2208-2218.

Ding, J., Sum, W.S., Sabesan, R., Leen, S.B., McColl, I.R. and Williams, E.J. (2007), "Fretting fatigue predictions in a complex coupling", *Int. J. Fatigue*, **29**, 1229-1244.

Duprat, D., Campassens, D., Balzano, M. and Boudett, R. (1996), "Fatigue life prediction of interference fit fastener and cold worked holes", *Int. J. Fatigue*, **18**(8), 515-521.

Finney, J.M. and Evans, R.L. (1997), "Extending the fatigue life of multi-layer metal joints", *Int. J. Fatigue*, **19**(3), 265-275.

Goranson, U.G. (1997), "Fatigue issues in aircraft maintenance and repairs", *Int. J. Fatigue*, **20**(6), 413-431.

Hibbit, D., Karlsson, B. and Sorensen, P. (2003), *ABAQUS User's Manual*, Version 6.4, USA HKS Inc.

Lacarac, V., Smith, D. and Pavier, M. (2001), "The effect of cold expansion on fatigue crack growth from open holes at room and high temperature", *Int. J. Fatigue*, **23**, 161-170.

Park, C.Y. and Grandt Jr. A.F. (2007), "Effect of load transfer on the cracking behavior at a countersunk fastener

hole”, *Int. J. Fatigue*, **29**, 146-157.

Shankar, K. and Dhamari, R. (2002), “Fatigue behavior of aluminum alloy 7075 bolted joints treated with oily film corrosion compounds”, *Mater. Des.*, **23**, 209-216.

Skorupa, M., Skorupa, A., Machniewicz, T. and Korbel, A. (2010), “Effect of production variables on the fatigue behaviour of riveted lap joints”, *Int. J. Fatigue*, **32**(7), 996-1003.

Smith, K.N., Watson, P. and Topper, T.H. (1970), “A stress-strain function for the fatigue of metals”, *J. Mater.*, **5**(4), 767-778.

Sum, W.S., Williams, E.J. and Leen, S.B. (2005), “Finite element, critical-plane, fatigue life prediction of simple and complex contact configurations”, *Int. J. Fatigue*, **27**(4), 403-416.

Yang, J.M., Her, Y.C. and Han, N.L. (2001), “Laser shock peening on fatigue behavior of 2024-T3 Al alloy with fastener holes and stopholes”, *Mater. Sci. Eng. A*, **298**, 296-299.

Zheng, X.L. (1986), “A further study on fatigue crack initiation life mechanical model for fatigue crack initiation”, *Int. J. Fatigue*, **9**(1), 17-21.